

Assessment of a vertical high-resolution distributed-temperature-sensing system in a shallow thermohaline environment

F. Suárez¹, J. E. Aravena², M. B. Hausner³, A. E. Childress², and S. W. Tyler¹

¹Department of Geological Sciences and Engineering, University of Nevada, Reno, USA

²Department of Civil and Environmental Engineering, University of Nevada, Reno, USA

³Graduate Program of Hydrologic Sciences, University of Nevada, Reno, USA

Received: 28 November 2010 – Published in Hydrol. Earth Syst. Sci. Discuss.: 5 January 2011

Revised: 25 March 2011 – Accepted: 26 March 2011 – Published: 30 March 2011

Abstract. In shallow thermohaline-driven lakes it is important to measure temperature on fine spatial and temporal scales to detect stratification or different hydrodynamic regimes. Raman spectra distributed temperature sensing (DTS) is an approach available to provide high spatial and temporal temperature resolution. A vertical high-resolution DTS system was constructed to overcome the problems of typical methods used in the past, i.e., without disturbing the water column, and with resistance to corrosive environments. This paper describes a method to quantitatively assess accuracy, precision and other limitations of DTS systems to fully utilize the capacity of this technology, with a focus on vertical high-resolution to measure temperatures in shallow thermohaline environments. It also presents a new method to manually calibrate temperatures along the optical fiber achieving significant improved resolution. The vertical high-resolution DTS system is used to monitor the thermal behavior of a salt-gradient solar pond, which is an engineered shallow thermohaline system that allows collection and storage of solar energy for a long period of time. The vertical high-resolution DTS system monitors the temperature profile each 1.1 cm vertically and in time averages as small as 10 s. Temperature resolution as low as 0.035 °C is obtained when the data are collected at 5-min intervals.

1 Introduction

Temperature fluctuations are a major driver of changes in natural and managed aquatic systems (Rosenzweig et al., 2007). In thermohaline aquatic environments such as estuaries or saline lakes, it is important to measure temperature on fine spatial and temporal scales to detect stratification or different hydrodynamic regimes. Spatial variability in shallow thermohaline systems can occur on vertical scales of centimeters and temporal variability occurs on time scales ranging from minutes to months, or even years (Anati and Stiller, 1991; Lorke et al., 2004; Lu et al., 2004; Kurt and Ozkaymak, 2006). Measuring temperature at these scales, especially when diurnal cycles need to be recorded over a long time period, can be difficult because of the cost involved (Branco et al., 2005) and other practical limitations, such as placing multiple sensors in a limited space. Multiple sensors need to be independently calibrated and may be subject to different intensities of drift in thermohaline environments (Bergman et al., 1985).

In the past, two methods have been used frequently to measure temperature gradients within the water column: first, a temperature sensor that can move vertically, and second, an array of fixed sensors at different depths. The moving sensor has the potential to mix the water column due to the motion of the sensors, obscuring the temperature gradients. Slow-moving sensors can be used to avoid this, but the temporal resolution of slower sensors is degraded. Arrays of sensors can introduce scatter into the data due to calibration differences and bias between the sensors, and have limited spatial resolution.



Correspondence to: F. Suárez
(suarezf@unr.edu)

Fiber-optic distributed temperature sensing (DTS) is an approach available to provide coverage in both space and time that can be used to continuously monitor real-time data in different environments. It was first developed in the 1980s (Dakin et al., 1985) and used in the oil and gas industry during the 1990s and early 2000s (Kersey, 2000); only since 2006 has it been widely used in hydrologic applications (Selker et al., 2006; Westhoff et al., 2007; Moffett et al., 2008; Tyler et al., 2009; Vogt et al., 2010). DTS technology uses Raman spectra scattering in a fiber-optic cable to measure temperatures along the cable length (this is referred to as the temperature trace). The ratio between the anti-Stokes and Stokes wavelengths of the Raman scattering is used to estimate the temperature along the fiber, and the location of the temperature measurement along the cable is calculated using the travel times of the incident and scattered lights. A detailed description of the theoretical basis of DTS systems is out of the scope of this work and can be found elsewhere (Rogers, 1999; Selker et al., 2006). Commonly available DTS systems can achieve a temperature resolution as fine as 0.01 °C (using 30-min integration-time intervals) with typical spatial and temporal resolutions of 1–2 m and 10–60 s, respectively, for cables up to 10 km (Selker et al., 2006). However, there are hydrologic environments such as shallow (<2 m deep) lakes or ponds where thermal observations at smaller vertical scales are required (Losordo and Piedrahita, 1991; Branco and Torgersen, 2009; Suárez et al., 2010a). This has resulted in the development of vertical high-resolution DTS systems.

The pioneering of a vertical high-resolution DTS system for hydrologic applications was presented by Selker et al. (2006). They monitored temperatures on a glacier and in a lake using an optical fiber wrapped around a 75 mm diameter 2 m length polyvinyl chloride (PVC) pole. Two platinum resistance thermistors (PT100), located at the top and bottom of the pole, were used to calibrate the temperature measurements along the optical fiber. This DTS system achieved a vertical spatial sampling resolution of 0.4 cm and a temperature resolution of 0.05 °C when 2 min integration intervals were used. Radiative heating on the pole had a profound impact on the air measurements above the glacier (Huwald et al., 2009). In the lake, where the water column was strongly mixed by the presence of waves during overcast conditions, radiative heating of the DTS pole was not observed. As the main purpose of the work performed by Selker et al. (2006) was to demonstrate the potential of DTS methods, only limited efforts were made to quantitatively assess the limitations of their DTS system. For example, having only two points of independent temperature measurements along the DTS pole may result in lower temperature accuracy along the optical fiber than that achieved with longer sections of cable at known temperature. Recently, Vogt et al. (2010) constructed a high-resolution DTS vertical temperature profiler to estimate seepage rates in a losing reach of a river. A fiber-optic cable was wrapped around a 51 mm diameter

1.9 m length PVC piezometer tube. The calibration of their DTS system was performed in the laboratory before field installation with two reference sections at two known temperatures. According to their manufacturer specifications, a temperature resolution of at least 0.11 °C should be achieved for cables shorter than 2 km when 10 min integration intervals were used. Although they were able to study groundwater and surface water interactions, deviations occurred due to calibration and signal noise of the DTS as well as solar radiation heating the DTS pole when the river stage was very low.

With their spatial and temporal resolution, DTS methods offer significant advantages over traditional measurement systems in natural or managed thermohaline environments. Fibers are low cost, with no issues of bias or fluid column disturbance, and can be made completely non-corroding. Radiation effects are similar to traditional sensors (Neilson et al., 2010). Nonetheless, DTS methods have complications and limitations that must be understood and assessed in order to achieve improved resolution. For instance, accuracy and precision of DTS systems depend on the fraction of incident light that is backscattered in the optical fiber and thus, one of the main limitations of DTS systems is low signal strength. Hence, care must be taken to avoid signal strength reductions, and evaluation of accuracy and precision of DTS systems is necessary for each installation. Also, DTS systems must be calibrated for differential attenuation of the anti-Stokes and Stokes intensities along the cable as well as instrument sensitivity and drift. Previous DTS investigations in hydrological or environmental applications have never presented the equations that DTS systems use for temperature estimation or temperature calibration. Few investigations in the field of light physics have derived the governing equation for temperature estimation along the fiber (Farahani and Gogolla, 1999; Yilmaz and Karlik, 2006), but their notation is inconsistent and some parameters have not been clearly defined. Therefore, temperature estimation (or calibration) in fiber-optic DTS systems still remains unclear.

The main objectives of this work are to present a method for using DTS technology to obtain more reliable temperature data and to assess the limitations of the technology. In particular, this study quantitatively assesses the performance of a vertical high-resolution DTS system, similar to that first presented by Selker et al. (2006), that is being used to monitor temperatures in a shallow thermohaline system. The evaluation of accuracy and precision is described and the selection between single- and double-ended measurements (described below) is discussed. A new method to manually calibrate the temperatures along the fiber is presented, and the notation and definition of the parameters needed to calibrate the temperature along the optical fiber is clarified. Although this study focuses on vertically wrapped fibers, the assessment presented here is also valid for DTS systems with linear arrangement of the fiber. A second objective is to demonstrate the utility of this method to accurately

monitor temperatures in a salt-gradient solar pond (hereafter, the term salt-gradient will be dropped), an engineered shallow thermohaline system that consists of three distinctive layers (Suárez et al., 2010b): the upper convective zone, a thin layer of cooler, less salty water; the non-convective zone, which has gradients in temperature and salinity; and the lower convective zone, a layer of high salinity brine (near saturation) where temperatures are the highest. In particular, temperatures collected with electrical conductivity (EC) probes are used to compare the DTS measurements within the solar pond, and the effects of radiative heating on the optical fiber are evaluated.

2 Materials and methods

2.1 Vertical high-resolution DTS system

A vertical high-resolution DTS system was constructed consisting of a vertical high-resolution pole, a DTS instrument, two water baths at different temperatures (for calibration purposes), and a fiber-optic cable that connects all the components. The total length of the fiber-optic cable was ~ 400 m, with ~ 200 m used in the vertical high-resolution DTS pole, ~ 50 m used in each bath, and the remainder used to connect the DTS instrument with each component of the system.

2.1.1 Vertical high-resolution DTS pole

A vertical high-resolution DTS pole (Fig. 1a) was constructed by carefully wrapping a duplex (i.e., two fibers in one cable) multi-mode fiber-optic cable (AFL Telecommunications, Spartanburg, SC) around a 51 mm diameter PVC pipe ~ 1.3 m in length. The geometric characteristics of the fiber-optic cable and the PVC pipe allowed 1 m of cable to occupy 1.1 cm of pipe length. The fiber-optic cable consists of a plastic jacket tube filled with a thixotropic gel and two non-armored optical fibers with core and cladding diameters of 50 and 125 μm , respectively. The cable was secured to the pipe using a white heat-shrink plastic, which is likely to reduce radiative heating. The interior of the PVC pipe was filled with insulating foam to prevent convective heat flow inside the pipe itself. The result was an easily handled, chemically inert, light-weight pole, resistant to the corrosive environment of hot saline water. The two optical fibers were fused at the end of the cable to create a loop of a single cable with both ends connected to the DTS instrument. This allowed access to the entire optical path of the cable via connection of the DTS to either end of the fiber.

2.1.2 DTS instrument

The vertical high-resolution DTS pole was connected to a SensorNet Sentinel DTS instrument (SensorNet Ltd., Herthfordshire, England), which according to the manufacturer,

has a temperature resolution <0.01 $^{\circ}\text{C}$ (60 min integration intervals) and a spatial sampling interval of 1.015 m, when cables shorter than 5 km are used. A four-channel multiplexer was employed to allow the use of single- or double-ended measurements. Single-ended measurements refer to temperatures estimated from light transmission in only one direction along the fiber. These measurements provide more precision near the instrument and degrade with distance due to the energy loss along the fiber length. Double-ended measurements refer to temperatures estimated from light transmission in both directions along the fiber. In double-ended measurements, the temperature is estimated using single-ended measurements made from each end of the optical fiber and accounts for spatial variation in the differential attenuation of the anti-Stokes and Stokes signals, which often occurs in damaged or strained fibers. This results in a signal noise more evenly distributed across the entire length of the cable, but uniformly greater than that obtained in a single-ended measurement (Tyler et al., 2009).

2.1.3 Calibration and verification

Here, we present a new method to calibrate temperatures along the fibers for single-ended measurements. We recognize that it is also necessary to present a calibration method for double-ended measurements, especially for damaged or strained cables that have spatially variable differential attenuation. However, because the differential attenuation along the length of our cable was fairly constant and due to the complexity of this method, it is out of the scope of this work and it remains to be a topic that will continue to be addressed in future investigations.

The temperature in an optical fiber can be estimated by (Farahani and Gogolla, 1999; Yilmaz and Karlik, 2006):

$$T(z) = \frac{\gamma}{\ln[C] - \ln[R(z)] + \Delta\alpha z} \quad (1)$$

$$R(z) = I_{\text{aS}}(z)/I_{\text{S}}(z) \quad (2)$$

where $T(z)$ is the temperature (K) at a distance z (m) along the fiber; $\gamma = \Delta E/k$ (K), where ΔE (J) represents the difference in molecular energy states that drive Raman scattering and k (J K^{-1}) is the Boltzmann constant; C (–) is a calibration parameter that depends on the wavelength and frequency of the incident laser, the backscattered Raman signals, the instrument's photon detector, and the operating conditions of the DTS instrument; $R(z)$ (–) is the ratio between the anti-Stokes and Stokes intensities, $I_{\text{aS}}(z)$ and $I_{\text{S}}(z)$ (arbitrary units), respectively; and $\Delta\alpha = \alpha_{\text{S}} - \alpha_{\text{aS}}$ (m^{-1}) is the differential attenuation of the backscattered Stokes and anti-Stokes intensities. Assuming that $\Delta\alpha$ is not spatially dependent, two methods can be used to calibrate the temperatures. First, temperatures can be estimated using the software provided by DTS manufacturers (this is referred to as manufacturer-internal calibration). This calibration method

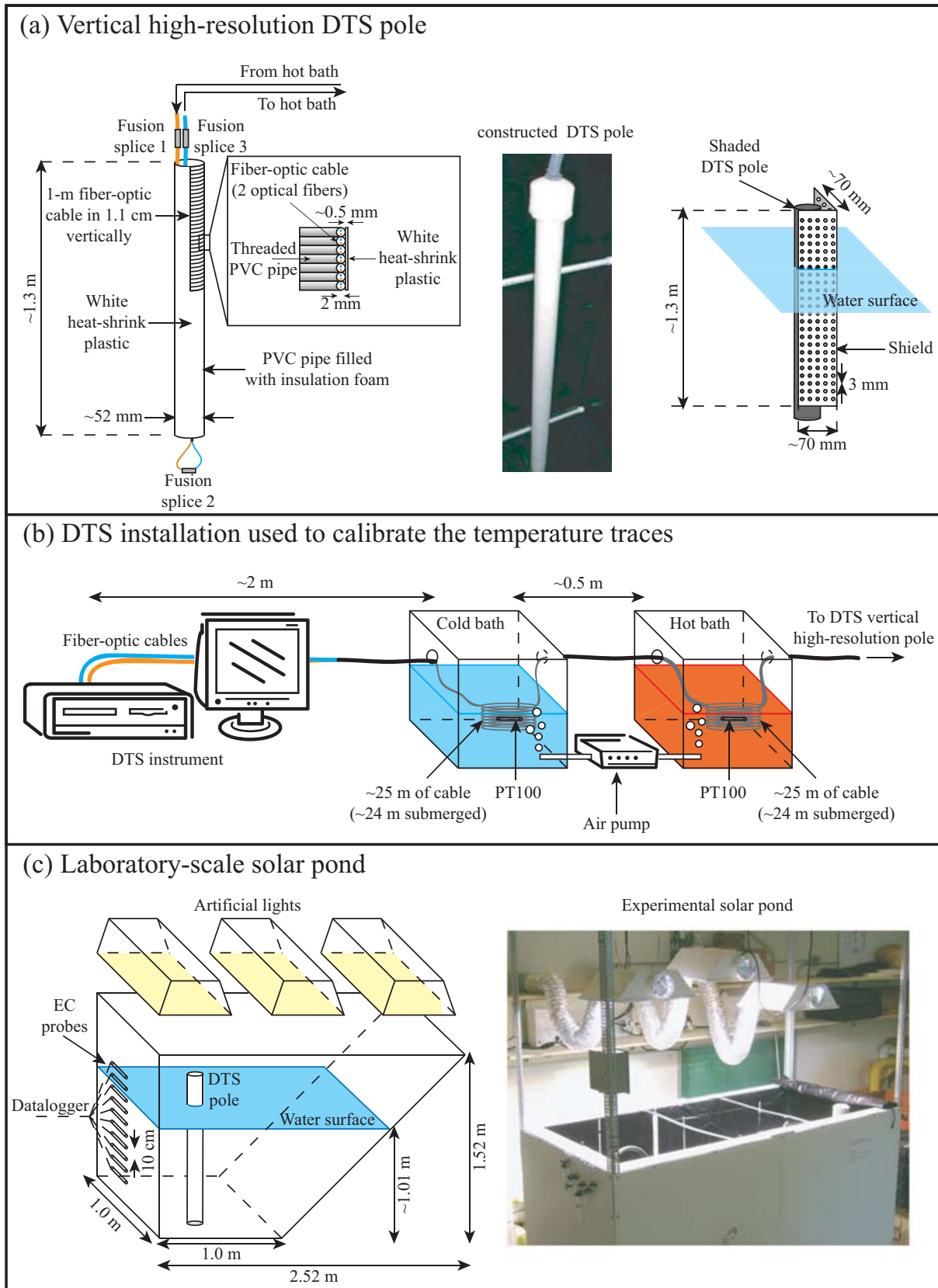


Fig. 1. Diagrams of the (a) DTS pole, (b) DTS installation, and (c) experimental solar pond.

generally assumes that the constant γ is known ahead of time and thus, the calibration requires two points (or sections) of known temperature to determine the constants $\Delta\alpha$ and C . This calibration method has been widely used in previous hydrologic investigations (Selker et al., 2006; Westhoff et al., 2007; Tyler et al., 2009). Second, temperatures can be calibrated manually using Eq. (1) (this is referred to as extended calibration). This calibration method assumes that the constants $\Delta\alpha$, γ and C are not known ahead of time. As a result, this calibration method requires three points (or sections) of known temperature. Two of these points can be at the same temperature and the other one at a different temperature. In the extended calibration method, two points held at the same temperature on the optical fiber are used to calculate $\Delta\alpha$. If z_1 and z_2 are the positions of these points, Eq. (1) yields:

$$\Delta\alpha = \frac{(\ln [R(z_1)] - \ln [R(z_2)])}{(z_1 - z_2)} \quad (3)$$

Once $\Delta\alpha$ is known, the values of C and γ are calculated using Eq. (1) at two points on the fiber held at different temperatures:

$$\ln [C] = \frac{(\ln [R(z_1)] - \Delta\alpha z_1) T(z_1)}{T(z_1) - T(z_3)} \dots - \frac{(\ln [R(z_3)] - \Delta\alpha z_3) T(z)}{T(z_1) - T(z_3)} \quad (4)$$

$$\gamma = (\ln [C] - \ln [R(z_1)] + \Delta\alpha z_1) T(z_1) \quad (5)$$

where z_3 is the position of a point on the fiber that has different temperature than that at positions z_1 or z_2 . When sections (instead of points) of known temperature are used to estimate the calibration parameters, the differential attenuation is calculated using the mean value of the $\Delta\alpha$ of contiguous points within the section, then C and γ are estimated using Eqs. (4) and (5). After the values of $\Delta\alpha$, C and γ are known, Eq. (1) is used to calculate the temperatures along the entire fiber. Calibration parameters ($\Delta\alpha$, C and γ) are recalculated for each time-step and are assumed to be uniform over the entire fiber length.

Two water baths were used as known-temperature reference sections to calibrate and verify the temperature readings of the DTS system (Fig. 1b). The first 25 m of cable were placed in a room-temperature water bath (cold bath) and were used to calibrate the temperature along the fiber. A four-wire 100-Ohm platinum resistance thermistor (PT100, $\pm 0.1^\circ\text{C}$) was positioned in the cold bath. The next 25 m of cable were placed in a microprocessor-controlled water bath (Precision 280, Thermo Electron Corporation, Waltham, MA) at a constant temperature of $\sim 60^\circ\text{C}$ (hot bath). A second PT100 thermistor ($\pm 0.1^\circ\text{C}$) was placed in the hot bath to verify the calibrated DTS readings. Air was circulated in both water baths to insure well mixed, isothermal conditions. The PT100 thermistors were previously calibrated using an NIST-traceable VWR thermometer ($\pm 0.05^\circ\text{C}$; Control Company, Friendswood, TX).

2.1.4 Resolution and repeatability

Spatial resolution is typically defined by DTS manufacturers as the length of cable required to show 80% of the temperature change between two known temperatures. To evaluate the spatial resolution of the DTS system, the step change in temperature between the cold and hot baths was analyzed. To evaluate the temporal resolution, a location on the optical fiber was monitored. When a fast and significant change in temperature occurred, the response time of the system was recorded and the temporal resolution was determined.

Repeatability refers to the agreements between successive measurements carried out under the same conditions. Spatial repeatability was quantified during a single trace by the standard deviation of consecutive temperature measurements over a given length of fiber that is at uniform temperature (Tyler et al., 2009). Temporal repeatability was quantified in a single point of the trace that was at a constant temperature by calculating the standard deviation of consecutive temperature measurements over a given time period.

2.1.5 Single- and double-ended measurements

The effect of single- and double-ended measurements on the temperature measurements was evaluated by comparing the temperature readings in the hot bath. In addition, the effect of temporal integration was also studied. Different combinations of measurements (single- and double-ended) and integration times were evaluated.

2.2 Evaluation of the vertical high-resolution DTS system in an experimental solar pond

A laboratory-scale experimental solar pond (Fig. 1c) was used to test the vertical high-resolution DTS system. To mimic the sunlight spectrum, three high-intensity-discharge lamps were installed over the pond. Each lamp consists of a 1000 W dual arc tube with two simultaneously operating arc tubes of metal halide and high pressure sodium with a wavelength range between 350 and 900 nm. Net radiation was measured ~ 10 cm above the water surface using a net radiometer (Q-7.1, Campbell Sci., Logan, UT). Incoming and reflected shortwave radiation were also measured ~ 10 cm above the water surface using two pyranometers (LP02, Hukseflux, Delft, The Netherlands). These data were collected using a datalogger (CR23X, Campbell Sci., Logan, UT) at 5 min intervals. Temperature and EC within the water were measured at ten points using EC electrodes (SK23T, Van London-pHoenix Company, Houston, TX) with automatic temperature compensation. Nine of the electrodes were made of glass and one of epoxy. The epoxy electrode replaced a glass electrode that broke during installation. A modular multi-channel datalogger (D230, Consort, Turnhout, Belgium) was used to record the data from the EC electrodes at 5 min intervals.

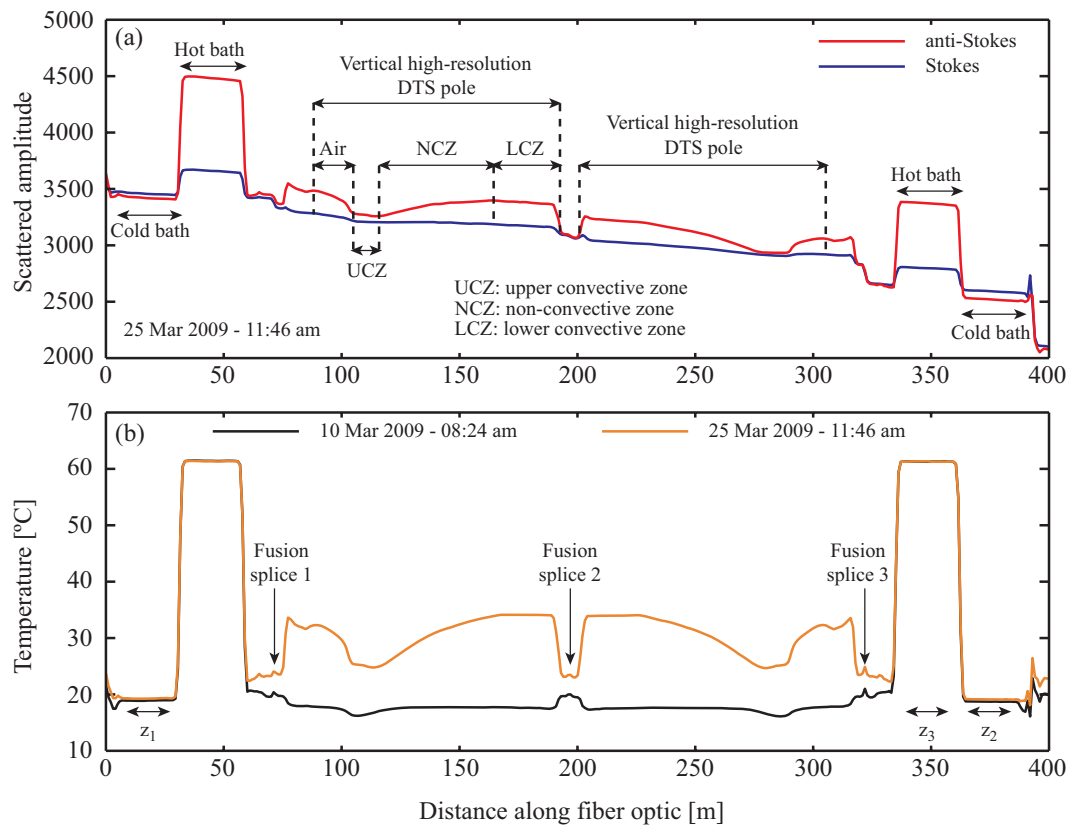


Fig. 2. (a) Typical Raman-scattering traces obtained during the experiment show the impact of temperature on the anti-Stokes and Stokes signals. Locations of the system components (cold and hot baths, vertical high-resolution DTS pole) are also shown. (b) Typical temperature traces measured during the experiment (obtained using the manufacturer-internal calibration method). The black line was obtained at the beginning of the experiment and the orange line was obtained after 15 days.

The lower 50 cm of the solar pond (i.e., the lower convective zone) were filled with a 20 wt% sodium chloride (NaCl) solution. Then, eight layers of successively lower concentrations were added up to an elevation of 90 cm measured from the bottom of the solar pond (i.e., the non-convective zone). Each layer had a NaCl concentration that was 2.2% lower than that of the previous layer. The final layer (i.e., the upper convective zone) was filled with tap water. The average water level in the solar pond was 101 cm (measured from the bottom), but the actual level varied from 98 to 103 cm due to evaporation and freshwater resupply. The average water level was used to calculate depths within the solar pond throughout the experiment (regardless that the true water level varied). The solar pond was covered tightly and allowed to sit for three days after filling. Then, the pond was typically exposed to the artificial lights 12 h per day (from 06:00 a.m. to 06:00 p.m. with the exception of the first day that was from 09:00 a.m. to 06:00 p.m.) and its thermal response was monitored using 5 min integration-time intervals.

In a separate investigation to assess the impact of radiative heating on the DTS pole, the lights over the pond were operated continuously. When the solar pond was close to

thermal steady state, the DTS pole was shaded using a white expanded-foam PVC shield (Fig. 1a). Holes were made in the shield to allow air (above the water surface) and water to move across it. The DTS pole was covered for approximately 60 min until a new steady state was reached. After this, the DTS pole was uncovered and temperatures were recorded using 10 s integration-time intervals until the initial value was reached.

3 Results and discussion

3.1 Vertical high-resolution DTS system

Typical Raman-scattering and temperature traces obtained during the experiment are presented in Fig. 2. Figure 2a shows the scattered anti-Stokes and Stokes signals along the fiber optic cable, the location of the components of the system (cold and hot bath, vertical high-resolution DTS pole), and the location of the distinct layers inside the solar pond. Figure 2b shows typical calibrated-temperature traces obtained during the experiment, and the locations where the

cable was fused. The temperature traces are symmetrical because the two fibers within the cable were fused at the end (fusion splice 2) to create a single loop. Figure 2 also shows how the temperature along the optical fiber affects the anti-Stokes and Stokes signals. As expected, the anti-Stokes signal is strongly dependent on the temperature along the fiber while the Stokes signal is weakly dependent on the temperature.

3.1.1 Calibration and verification

Figure 3a shows a comparison of the temperatures measured in the cold bath by the PT100 and by the DTS system. The DTS temperatures were calibrated using the manufacturer-internal calibration. These temperatures are expected to be equal because the DTS instrument uses the temperature measured in the cold-bath PT100 to correct the temperature measurements along the entire optical fiber. A normal probability plot (inset of Fig. 3a) shows that the difference between the DTS and PT100 temperatures follows a standard normal distribution (i.e., $\sim N(0, 1)$). Thus, these temperature differences are verified to be independent and could be considered as random noise with 95% confidence (Box et al., 2008).

The manufacturer-internal-calibrated DTS readings were verified by comparing the DTS and the PT100 measurements in the hot bath, as shown in Fig. 3b. The temperatures of both instruments are in agreement, although their differences have more variability than those measured in the cold bath. However, a normal probability plot shows that these temperature differences are also $\sim N(0, 1)$. Thus, random noise in the DTS system is the main reason for the observed differences, with a 5% significance level (Box et al., 2008). Statistically, the DTS and the thermistor measure the same temperature, verifying the readings of the DTS system.

To illustrate the extended calibration method, single-ended traces of the anti-Stokes and Stokes intensities were used to estimate the temperatures along the optical fiber. These temperatures were compared to the manufacturer-internal-calibrated temperatures. The mean value of the $\Delta\alpha$ was calculated from two sections on the optical fiber held at the same temperature (between 10 and 25 m and between 370 and 385 m, in the cold bath at $\sim 19.6^\circ\text{C}$, as shown in Fig. 2). The values of C and γ were calculated from two points on the fiber held at different temperatures ($z_1 = 17.5$ m at $\sim 19.6^\circ\text{C}$ in the cold bath and $z_3 = 347.5$ m at $\sim 61.5^\circ\text{C}$ in the hot bath). Figure 3c compares manufacturer-internal- and extended-calibrated temperatures within the solar pond. Generally, these calibrated temperatures differ in less than 0.1°C in the solar pond. The root mean square error (RMSE) of the points of known temperature along the cable was used to determine the goodness of the agreement between these calibrations. The extended-calibrated temperatures (RMSE = 0.05°C) are closer than the manufacturer-internal-calibrated temperatures (RMSE = 0.25°C) to the independent measures of temperature of the baths. This occurred

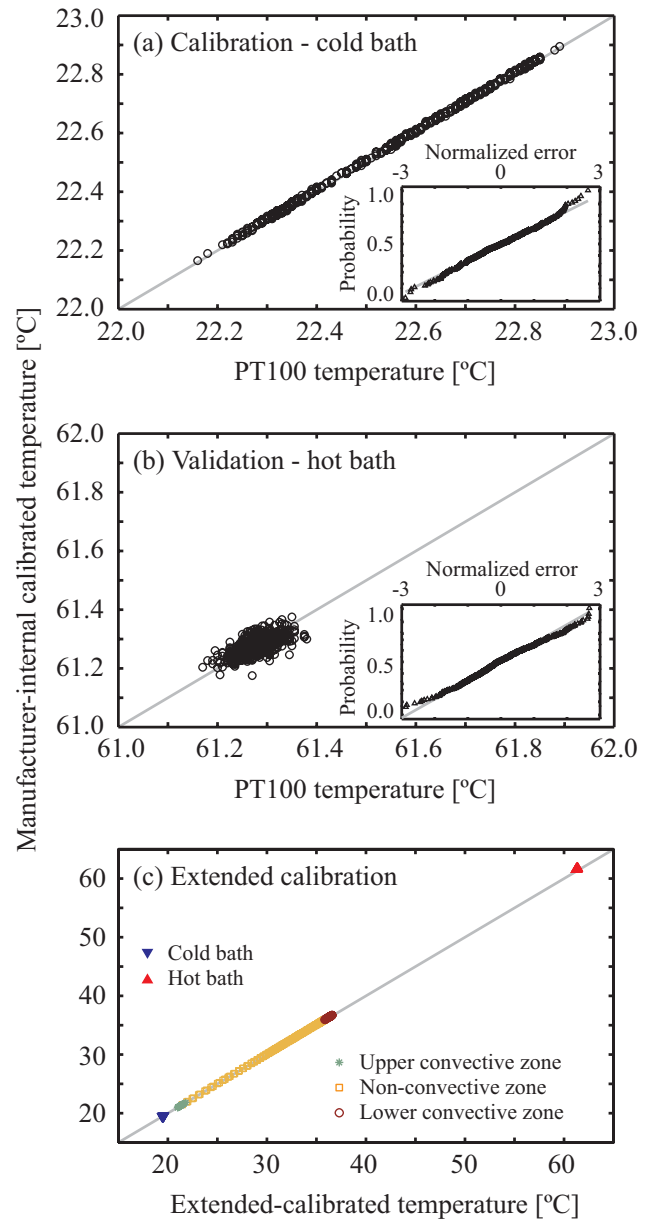


Fig. 3. (a) The DTS system is calibrated by comparing the PT100 temperature measurements with the DTS manufacturer-internal calibrated temperatures in the cold bath. (b) The DTS system is validated in the hot bath. (c) Extended- and manufacturer-internal calibrated temperatures are compared.

because manufacturer-internal-calibrated temperatures were estimated by varying two calibration parameters ($\Delta\alpha$ and C), while in the extended-calibrated temperatures three calibration parameters ($\Delta\alpha$, C and γ) were allowed to vary. Thus, manual post-processed data resulted in a more robust and usable data set.

The length of the known-temperature section and the selection of z_1 and z_3 may have an impact on the quality of the calibration. A sensitivity analysis showed that the effect

Table 1. Sensitivity analysis of the extended calibration for different lengths (L) of the calibration sections. RMSE and σ correspond to the root mean square error and the standard deviation of the extended-calibrated temperatures in the known-temperature sections.

L [m]	RMSE [°C]	σ [°C]
1	2.077	0.051
5	1.532	0.044
10	0.556	0.038

of the selection of z_1 and z_3 on quality of the calibration is negligible compared to the effect of the length of the known-temperature section (data not shown). Table 1 show that both the RMSE and the standard deviation of the extended-calibrated temperatures in the calibration baths are reduced as the length of the calibration section is increased. Thus, longer calibration sections are recommended for improved temperature resolution.

3.1.2 Resolution and repeatability

The spatial resolution was evaluated using the step change in temperature between the cold and hot baths. Utilizing 15 days of data (4495 temperature traces), it was found that the mean spatial resolution of the DTS system was 2.056 ± 0.047 m, which is twice that reported by the manufacturer. The results obtained here and in a previous study (Tyler et al., 2009) suggest that spatial resolution is at least two times the sampling resolution of the instrument. The temporal resolution of the high-resolution DTS pole was evaluated at ~ 1 cm above the air-water interface. An integration time of 10 s was utilized. Before the lights were turned on, a constant temperature of 24.223 ± 0.096 °C was monitored. After the lights were turned on, a significant and fast change in temperature (>4 °C in less than 5 min) was observed. The DTS system took less than 40 s to register an increase in temperature larger than $2\sigma = 0.192$ °C. Thus, the temporal resolution of the DTS system was ~ 40 s with 95% confidence.

Spatial repeatability was quantified during a single trace in the hot bath. The average temperature was 61.429 ± 0.014 °C. This is a very good spatial repeatability that is much better than that obtained in previously reported DTS experiments (Tyler et al., 2008, 2009). Temporal repeatability was also evaluated in the hot bath. The PT100 reported an average temperature of 61.333 ± 0.120 °C, while that reported by DTS system was 61.410 ± 0.121 °C. This suggests that actual variability of the hot bath controls the repeatability of the DTS measurement.

Table 2. Comparison between single-ended (SE) and double-ended (DE) measurements in the hot bath (obtained using the manufacturer-internal calibration method). T is average temperature and σ is standard deviation.

Integration time [s]	T_{SE} [°C]	σ_{SE} [°C]	T_{DE} [°C]	σ_{DE} [°C]
20	61.419	0.103	61.322	0.112
120	61.612	0.046	61.321	0.069
300	61.618	0.035	61.261	0.055

3.1.3 Single- and double-ended measurements

Selection of single- or double-ended measurements needs to be analyzed because it can result in different degrees of accuracy and temperature resolution. While single-ended measurements provide more precision near the instrument, double-ended measurements allow the users to accurately derive temperatures from fibers with spatial variation in the differential attenuation of the backscattered signals, which typically occurs in damaged or strained fibers.

As shown in Table 2, as the integration time increases the standard deviations of both single- and double-ended measurements decrease. For all the integration times, single-ended measurements show smaller standard deviation than double-ended measurements. An integration time of 300 s showed spatial repeatability (standard deviations) of 0.035 and 0.055 °C in the hot bath for single- and double-ended measurements, respectively. This integration time was long enough to provide good temperature resolution and short enough to monitor the transient phenomena and the physics of solar ponds. These results show that the DTS system is able to resolve temperatures with very small variability using both types of measurements. In this experiment the cables were less than one tenth the instrument's range, so noise levels were roughly the same in single- and double-ended measurements for equivalent integration times. Somewhat surprisingly, the expected decrease in standard deviation with the square-root of the integration time did not hold for the double-ended measurements, which showed less than half the expected improvement in precision, while the single ended measurements achieved about 70% of the theoretically anticipated improvement. A frequency stability analysis, using the modified Allan variance method (Rubiola, 2005), showed the presence of a combination of white and flicker noises. Flicker noise (also known as $1/f$ or pink noise) is ubiquitous in physics (Lawrence et al., 1987; Kaulakys and Alaburda, 2009) and is expected in technologies that use weak optical signals such as Raman-scattering applications (McDowell et al., 2008). When white and flicker noise are combined, the signal-to-noise ratio of optical instruments is smaller than that obtained when only white noise is present.

As a result, the expected decrease in standard deviation due to increasing averaging time is also smaller.

3.2 Evaluation of the vertical high-resolution DTS system in an experimental solar pond

The thermal evolution of the water column and the air above it is presented in Fig. 4a. The night surface cooling, the non-convective zone stratification, and the warming of the lower convective zone are observed at high spatial and temporal resolutions. To the best of our knowledge, this is the first time that temperatures have been reported at such high spatial and temporal resolution in solar ponds (Lu et al., 2004; Kurt and Ozkaymak, 2006). This spatial and temporal resolution of the temperature observations is not only a tool for monitoring temperatures at near real-time but also could become a tool for decision-making. For instance, at the beginning of the experiment, no water was added to the surface of the pond and evaporation decreased the water level. After one week, the DTS system showed air temperatures at more than 5 cm depth; for this reason it was decided to resupply freshwater at the surface of the pond. The timing of the first resupply is clearly observed in Fig. 4a.

Figure 4b shows the thermal evolution at different depths within the solar pond. It can be seen that during the first days of the experiment, the upper convective zone (red and black lines) is stratified during the day and completely mixed during the night. After one week, the upper convective zone is always completely mixed. Figure 4b also shows that the non-convective zone strongly stratifies and that temperatures in the middle of this zone (orange and gold lines) are less affected by daily fluctuations. The close-up in Fig. 4b shows that the lower convective zone is completely mixed during the day but stratified at night because heat is lost through the non-convective zone as well as through the bottom and sides of the experimental solar pond. These heat losses can be easily assessed using the DTS system (e.g., by evaluating the thermal gradient measured near the bottom). For a detailed interpretation of the physics observed in this experiment, the reader is referred to the work of Suárez et al. (2010c).

Figure 5 shows the temperature profiles using the DTS system and using EC probes for different days of the experiment. The initial design of the experiment located the interface between the non-convective and the lower convective zones at 0.5 m depth. On the morning of 6 March 2009, only the lower convective zone of the solar pond was filled. At this time, the temperature profile measured with the DTS system showed an essentially uniform water temperature below the air boundary layer that begins at the water surface. The spatial resolution obtained with the vertical high-resolution DTS system cannot be readily achieved with a fixed array of thermocouples; or by using a DTS system with a linear arrangement of the fiber. The DTS method was also found to be less affected by the aggressive saline environment. For instance, on the morning of 6 March, though the EC probes showed

the same spatial trend as the DTS system, the submerged EC probes exhibited higher temperatures than those measured by the vertical high-resolution DTS system. On the other hand, the EC probes above the water surface confirmed that the air temperature measured with the DTS pole was properly reported by the DTS instrument. It appears that the brine caused an offset of $\sim 0.5^\circ\text{C}$ in the submerged EC probes. Electrode drift due to the saline environment (Bergman et al., 1985) could have been one of the reasons for this offset. The EC probe located at ~ 0.4 m depth, which was the single probe made of epoxy, consistently reported lower temperatures than the other probes. This clearly demonstrates the disadvantage of data scatter due to biases between sensors when using a fixed array. In addition, the EC probe located at ~ 0.75 m depth did not record both temperature and EC throughout the experiment.

The filling of the pond was completed the afternoon of 6 March and the pond was tightly covered to avoid heat transfer between the water and the ambient air. On 9 March, the pond was left uncovered during the night and the experiments started at 09:00 a.m. the morning of 10 March. At 08:54 a.m. (6 min before turning on the lights for the first time), the effect of surface cooling at night is clearly visible in both the DTS system and the EC probes (yellow data in Fig. 5). By 13 March, the DTS system already shows that the lower convective zone is completely mixed. Furthermore, the vertical high-resolution DTS system shows that the interface between the non-convective and lower convective zones is located deeper than the desired level (at ~ 0.65 m depth). This reduction of the lower convective zone occurred when constructing the salt gradient (Suárez et al., 2010c). If the temperatures measured with the EC probes are analyzed, the lower convective zone is not as clear as in the DTS measurements because almost all the data points along the water column are scattered between 23 and 24 $^\circ\text{C}$ (without considering the probe located at ~ 0.4 m depth). On 25 March, the DTS system shows that the temperature profile in the non-convective zone corresponds with the theoretical profile expected when a static fluid is absorbing energy, i.e., a non-linear gradient occurs when conduction is the main heat transfer mechanism and radiation produces internal heating of the fluid (Bejan, 2004). The temperatures measured by the EC probes show a slight curvature in the non-convective zone, but it is not clear if it is a constant temperature gradient or not. In Fig. 5, the gray-dashed line shows erosion of the lower convective zone observed using the DTS system. On 25 March, the DTS system shows the location of the interface between the non-convective and lower convective zones at ~ 0.7 m depth. Because of the poor spatial distribution of the EC probes, these sensors show the interface between the non-convective and lower convective zone at ~ 0.6 m depth.

The effect of radiative heating is shown in Fig. 6. The temperatures measured by the DTS system in the air above the water column and the temperatures in the upper convective zone were the ones most affected by radiation absorption,

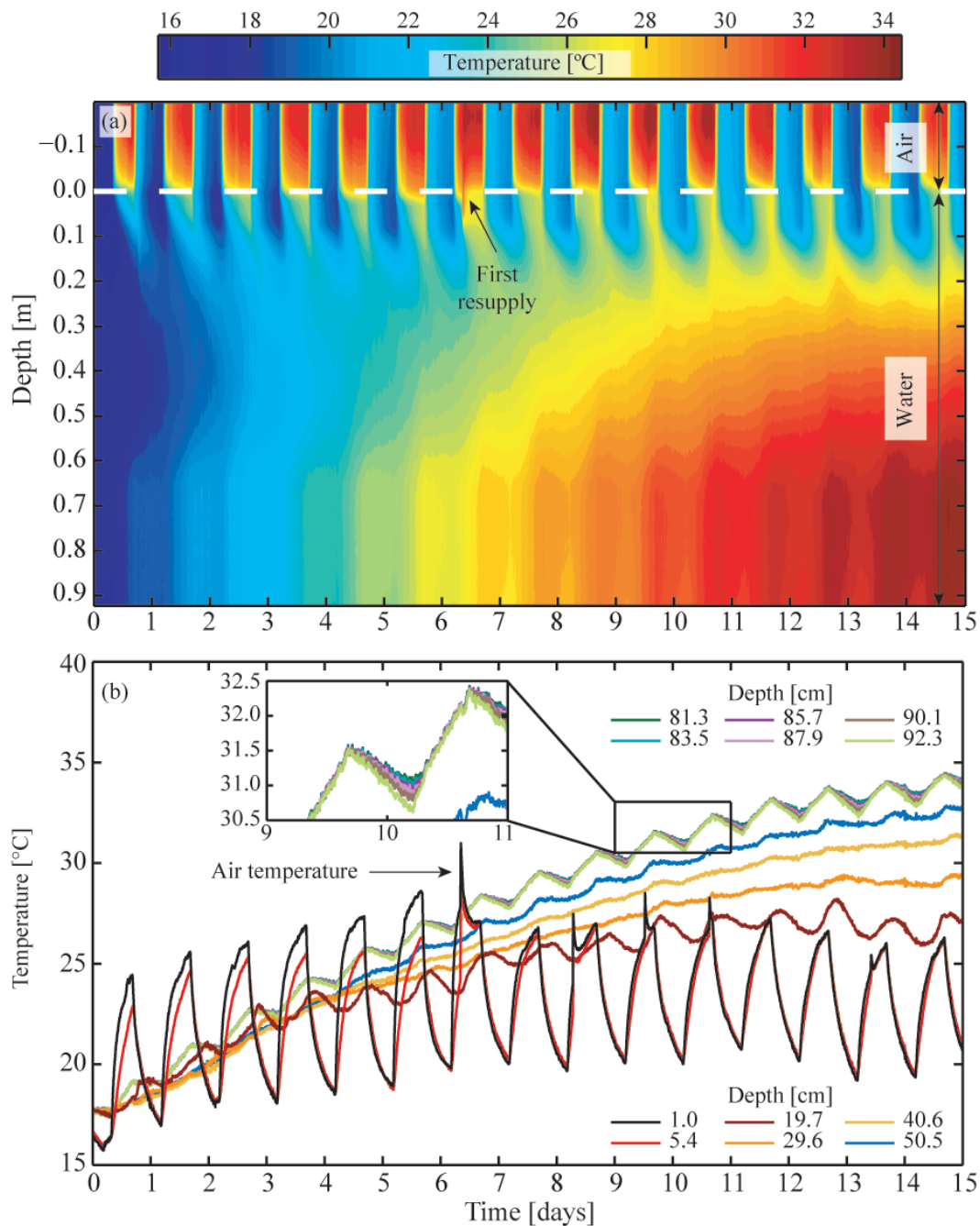


Fig. 4. (a) Thermal evolution of the water column and the air above it collected with the vertical high-resolution DTS system. (b) Time series of temperature at specific depths inside the solar pond. These measurements were obtained using the manufacturer-internal calibration method.

while the water temperatures below the upper convective zone were not affected when the DTS pole was shaded. As shown in Fig. 6a, after 20 min of covering the DTS pole, the temperature readings at 2.3 cm above the water level achieved a new steady-state. Here, the temperature readings were 0.7°C lower than those without the cover. Figure 6b shows the thermal profiles measured with the DTS system

for different times during the radiative heating experiment. When the DTS pole was covered, the air temperature profile changed from a non-linear shape into a more linear shape. This is expected in a static system that is not subject to internal heat generation (Bejan, 2004). Thus, when the DTS pole is not shielded, the curvature observed in the air temperature profile is due to absorption of radiation in the DTS pole.

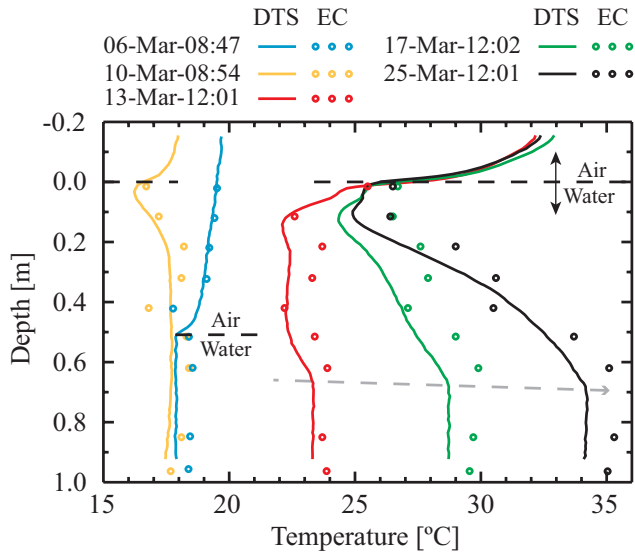


Fig. 5. Comparison of the temperature profile measured with the DTS system and with electrical conductivity (EC) probes. In the morning of 6 March the solar pond was filled to a depth of 0.50 m. These measurements were obtained using the manufacturer-internal calibration method.

In the upper convective zone, the temperature decreased by ~ 0.1 °C when the DTS pole was shielded. When the shield was removed, the temperature of this zone increased rapidly for the first 15 min until a new steady state was reached at the end of the experiment, demonstrating how radiation absorption in the DTS pole affects the temperature measurements at shallow depths.

Radiative heating of the DTS pole, for the radiation levels tested here (net radiation of 243 W m^{-2} at the water surface – limited by the intensity of the artificial lights), was significant only when air or shallow water were measured. Temperature measurements with the DTS pole between the water surface and 10 cm depth showed only an additional 0.1 °C that was attributed to radiation absorption. Peaks of natural solar radiation can be 3–4 times higher than the radiation levels tested here. Hence, the impact of solar radiation absorption on the DTS pole, as well as on other temperature sensors that are not shielded, may be important when water temperatures are being measured. The systems may be especially sensitive when water velocities are very small, i.e., when conduction is the dominant heat transfer mechanism, and when the magnitude of solar radiation is large (Huwald et al., 2009; Neilson et al., 2010). The impact of solar radiation absorption on fiber-optic cables can be reduced using reflective coatings or using shields to shade the cables. An optimal shield should minimize the radiation reaching the cable and the radiation absorbed by the shield, while maximizing the air or water flow around the cable (Richardson et al., 1999). If reflective coatings are used, care must be taken to not affect, i.e., warm, the surrounding environment (e.g., see Huwald et al., 2009).

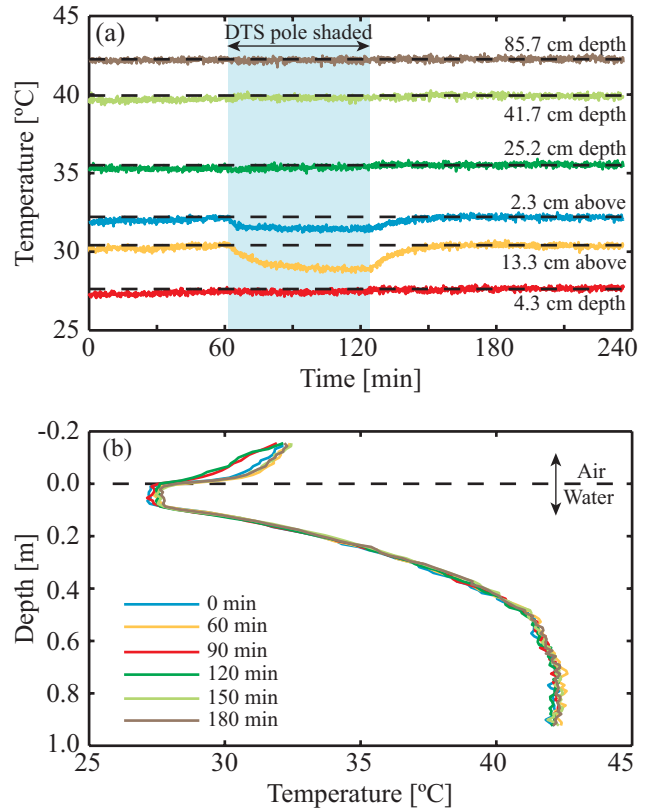


Fig. 6. Assessment of radiative heating of the DTS pole. (a) Thermal evolution at different depths in the water column and in the air. (b) Temperature profile measured with the DTS system at different times of the experiment. These measurements were obtained using a 10-s integration-time interval and using the manufacturer-internal calibration method.

4 Summary and conclusions

As temperature is a major driver of changes in natural and managed aquatic systems, there is a need to observe temperatures at high spatial and temporal resolutions. The vertical high-resolution DTS system provides a reliable method to monitor temperature in space and time, which is essential in many hydrological applications such as thermohaline environments. In addition, the presented DTS system overcomes the problems typical of methods used in the past such as drift due to corrosive environment. This is a major issue in thermohaline systems, particularly in solar ponds where the salinity approaches saturation.

This paper presented a methodology for calibration as well as for evaluation of spatial and temporal repeatability and resolution that helps to maximize the potential of the fiber-optic DTS technology for hydrologic applications. The extended-calibrated temperatures resulted in a more robust and usable data set than the manufacturer-internal calibrated-temperatures. The present DTS system monitored the temperature profile in a solar pond each 1.1 cm vertically and

in time averages as small as 10 s. Temperature resolution as low as 0.035 °C was obtained when the data were collected at 5 min intervals. It was found that the DTS system resolved temperatures with very small variability using either single- or double-ended measurements, and that the observed noise in the system could be due to a combination of white and flicker noise. Using the vertical high-resolution DTS system, stratification, mixing, interface erosion, and freshwater re-supply were observed in the solar pond at a resolution that is hardly achievable using traditional temperature sensors. In our experimental setup, radiation absorption was found to be significant only when air or shallow water temperatures were measured. However, it may be important in systems exposed to natural solar radiation.

Acknowledgements. The authors wish to thank the Department of Energy (DOE) for funding Grants DE-FG02-05ER64143 and 656-1769-01-NV-REC (Nevada Renewable Energy Consortium), and the National Science Foundation (NSF) for partial funding of this work by Award NSF-EAR-0929638. The authors greatly appreciate the support of Jeffrey Ruskowitz, the valuable input from John S. Selker, and the constructive suggestions of Martijn Westhoff, Hendrik Huwald (reviewers) and Ty Ferre (editor).

Edited by: T. P. A. Ferre

References

- Anati, D. A. and Stiller, M.: The post-1979 thermohaline structure of the dead-sea and the role of double-diffusive mixing, *Limnol. Oceanogr.*, 36, 342–354, 1991.
- Bejan, A.: *Convection Heat Transfer*, 3rd edition, John Wiley and Sons, Inc, New Jersey, 2004.
- Bergman, T. L., Incropera, F. P., and Stevenson, W. H.: Miniature fiber-optic refractometer for measurement of salinity in double-diffusive thermohaline systems, *Rev. Sci. Instrum.*, 56, 291–296, 1985.
- Box, G., Jenkins, G., and Reinsel, G.: *Time Series Analysis. Forecasting and Control*, 4th edition, John Wiley and Sons, Inc, New Jersey, 2008.
- Branco, B., Torgersen, T., Bean, J. R., Grenier, G., and Arbige, D.: A new water column profiler for shallow aquatic systems, *Limnol. Oceanogr. Meth.*, 3, 190–202, 2005.
- Branco, B. F. and Torgersen, T.: Predicting the onset of thermal stratification in shallow inland waterbodies, *Aquat. Sci.*, 71, 65–79, 2009.
- Dakin, J. P., Pratt, D. J., Bibby, G. W., and Ross, J. N.: Distributed optical fiber Raman temperature sensor using a semiconductor light-source and detector, *Electron. Lett.*, 21, 569–570, 1985.
- Farahani, M. A. and Gogolla, T.: Spontaneous Raman scattering in optical fibers with modulated probe light for distributed temperature Raman remote sensing, *J. Lightwave Technol.*, 17, 1379–1391, 1999.
- Huwald, H., Higgins, C. W., Boldi, M. O., Bou-Zeid, E., Lehning, M., and Parlange, M. B.: Albedo effect on radiative errors in air temperature measurements, *Water Resour. Res.*, 45, W08431, doi:10.1029/2008WR007600, 2009.
- Kaulakys, B. and Alaburda, M.: Modeling scaled processes and $1/f^\beta$ noise using nonlinear stochastic differential equations, *J. Stat. Mech.-Theory E.*, P02051, doi:10.1088/1742-5468/2009/02/P02051, 2009.
- Kersey, A. D.: Optical fiber sensors for permanent downwell monitoring applications in the oil and gas industry, *IEICE T. Electron.*, E83-C, 400–404, 2000.
- Kurt, H. and Ozkaymak, M.: Performance evaluation of a small-scale sodium carbonate salt gradient solar pond, *Int. J. Energ. Res.*, 30, 905–914, 2006.
- Lawrence, A., Watson, M. G., Pounds, K. A., and Elvis, M.: Low-frequency divergent X-ray variability in the Seyfert galaxy NGC4051, *Nature*, 325, 694–696, 1987.
- Lorke, A., Tietze, K., Halbwachs, M., and Wuest, A.: Response of Lake Kivu stratification to lava inflow and climate warming, *Limnol. Oceanogr.*, 49, 778–783, 2004.
- Losordo, T. M. and Piedrahita, R. H.: Modeling temperature variation and thermal stratification in shallow aquaculture ponds, *Ecol. Model.*, 54, 189–226, 1991.
- Lu, H. M., Swift, A. H. P., Hein, H. D., and Walton, J. C.: Advancements in salinity gradient solar-pond technology based on sixteen years of operational experience, *J. Sol. Energ.-T. ASME*, 126, 759–767, 2004.
- McDowell, E. J., Ren, J., and Yang, C.: Fundamental sensitivity limit imposed by dark $1/f$ noise in the low optical signal detection regime, *Opt. Express*, 16, 6822–6832, 2008.
- Moffett, K. B., Tyler, S. W., Torgersen, T., Menon, M., Selker, J. S., and Gorelick, S. M.: Processes controlling the thermal regime of saltmarsh channel beds, *Environ. Sci. Technol.*, 42, 671–676, 2008.
- Neilson, B. T., Hatch, C. E., Ban, H., and Tyler, S. W.: Solar radiative heating of fiber-optic cables used to monitor temperatures in water, *Water Resour. Res.*, 46, W08540, doi:10.1029/2009WR008354, 2010.
- Richardson, S. J., Brock, F. V., Semmer, S. R., and Jirak, C.: Minimizing errors associated with multiplate radiation shields, *J. Atmos. Ocean. Tech.*, 16, 1862–1872, 1999.
- Rogers, A.: Distributed optical-fibre sensing, *Meas. Sci. Technol.*, 10, R75–R99, 1999.
- Rosenzweig, C., Casassa, G., Karoly, D. J., Imeson, A., Liu, C., Menzel, A., Rawlins, S., Root, T. L., Seguin, B., and Tryjanowski, P.: Assessment of observed changes and responses in natural and managed systems, in: *Climate Change 2007: Impacts, Adaptation and Vulnerability. Contribution of Working Group II to the Fourth Assessment Report of the Intergovernmental Panel on Climate Change*, edited by: Parry, M. L., Canziani, O. F., Palutikof, J. P., and van der Linden, P. J., Cambridge University Press, 79–131, 2007.
- Rubiola, E.: On the measurement of frequency and of its sample variance with high-resolution counters, *Rev. Sci. Instrum.*, 76, 054703, doi:10.1063/1.1898203, 2005.
- Selker, J. S., Thevenaz, L., Huwald, H., Mallet, A., Luxemburg, W., van de Giesen, N. C., Stejskal, M., Zeman, J., Westhoff, M., and Parlange, M. B.: Distributed fiber-optic temperature sensing for hydrologic systems, *Water Resour. Res.*, 42, W12202, doi:10.1029/2006WR005326, 2006.
- Suárez, F., Tyler, S. W., and Childress, A. E.: A fully coupled, transient double-diffusive convective model for salt-gradient solar ponds, *Int. J. Heat Mass Tran.*, 53, 1718–1730, 2010a.

- Suárez, F., Tyler, S. W., and Childress, A. E.: A theoretical study of a direct contact membrane distillation system coupled to a salt-gradient solar pond for terminal lakes reclamation, *Water Res.*, 44, 4601–4615, 2010b.
- Suárez, F., Childress, A. E., and Tyler, S. W.: Temperature evolution of an experimental salt-gradient solar pond, *J. Water Climate Change*, 1, 246–250, 2010c.
- Tyler, S. W., Burak, S. A., Mcnamara, J. P., Lamontagne, A., Selker, J. S., and Dozier, J.: Spatially distributed temperatures at the base of two mountain snowpacks measured with fiber-optic sensors, *J. Glaciol.*, 54, 673–679, 2008.
- Tyler, S. W., Selker, J. S., Hausner, M. B., Hatch, C. E., Torgersen, T., Thodal, C. E., and Schladow, S. G.: Environmental temperature sensing using Raman spectra DTS fiber-optic methods, *Water Resour. Res.*, 45, W00D23, doi:10.1029/2008WR007052, 2009.
- Vogt, T., Schneider, P., Hahn-Woernle, L., and Cirpka, O. A.: Estimation of seepage rates in a losing stream by means of fiber-optic high-resolution vertical temperature profiling, *J. Hydrol.*, 380, 154–164, 2010.
- Westhoff, M. C., Savenije, H. H. G., Luxemburg, W. M. J., Stelling, G. S., van de Giesen, N. C., Selker, J. S., Pfister, L., and Uhlenbrook, S.: A distributed stream temperature model using high resolution temperature observations, *Hydrol. Earth Syst. Sci.*, 11, 1469–1480, doi:10.5194/hess-11-1469-2007, 2007.
- Yilmaz, G. and Karlik, S. E.: A distributed optical fiber sensor for temperature detection in power cables, *Sensor. Actuat. A-Phys.*, 125, 148–155, 2006.